High Temperatures-High Pressures, Vol. 48, pp. 253–277
Reprints available directly from the publisher
Photocopying permitted by license only
DOI: 10.32908/hthp.v48.648

Non-linear effects in the oscillating drop method for viscosity measurements

Rainer K. Wunderlich* and Markus Mohr

Institute for Functional Nanosystems
Ulm University, Albert-Einstein-Allee 47, D-89081 Ulm, Germany

Received: January 5, 2018; Accepted: November 28, 2018.

The contribution of non-linear fluid flow effects to the damping of surface oscillations in the oscillation drop method was investigated in a series of experiments in an electromagnetic levitation device installed on the International Space station, ISS-EML. In order to correctly evaluate the damping time constant from measured surface oscillation decays the effect of a modulated signal response on measured surface oscillation decay curves was investigated. It could be shown that various experimentally observed signal patterns could be well represented by a modulated response. The physical origin of such modulations is seen in rotation and precession. Over a temperature range of 220 K covered by different surface oscillation excitation pulses with an initial sample shape deformation of 5–10% the amplitude of surface oscillations as a function of time could be very well represented by a Lamb type damping with a temperature dependent viscosity. A direct comparison of surface oscillation decay times measured in the same temperature range but for different oscillation amplitudes showed no non-linear contribution to the damping time constant with a confidence level better 10%.

Keywords: oscillating drop method, viscosity, containerless processing, electromagnetic levitation, non-linear fluid flow effects

1 INTRODUCTION

Thermophysical properties of liquid metallic alloys are important input parameters for the modelling of industrial casting processes [1,2] and, more

*Corresponding author: rainer.wunderlich@uni-ulm.de

generally, for a better understanding of the properties of metallic liquids including the undercooled liquid phase [3]. Many alloys of industrial interest have high liquidus temperatures and exhibit a high dissolution reactivity in the liquid phase which makes thermophysical property measurements with classical methods where the liquid is in contact with a container difficult and results fraught with error. Examples are the γ-TiAl, the Ti6Al4V (wt%) or Zr-based alloys. As a consequence, containerless methods either in an electromagnetic (eml) [4, 5] or electrostatic levitation device (esl) [6, 7] are applied for thermophysical property measurements in the liquid phase.

Knowledge of the viscosity and its temperature dependence are essential for the simulation of fluid flow in various casting and liquid metal processing simulations. It is also of principal interest as a transport property of metallic glass forming liquids. The oscillating drop method applied either in an eml [8, 9, 10] or esl [11, 12] is the method of choice for the measurement of the viscosity and surface tension of high temperature reactive metallic alloys. In an eml a freely suspended liquid droplet is exposed to a short duration pulse of the em-heating field for the excitation of surface oscillations. Under ideal force free conditions, the absence of turbulence and a small initial deformation, the viscosity η can be evaluated from the damping time constant of the surface oscillations, k_{L}, according to the Lamb formula [13]:

$$\eta = \frac{3}{20\,\pi}\,\frac{M}{R_{\mathrm{o}}}\,k_{\mathrm{L}} \tag{1}$$

with M and R_{o}, the mass and equilibrium radius of the sample. Under the same conditions the surface tension, σ, is evaluated from the frequency of the surface oscillations, ν_{sc}, according to Rayleigh's formula [14]:

$$\sigma = \frac{3}{8}\,\pi\,M\nu_{\mathrm{sc}}^{2} \tag{2}$$

Regarding the surface tension, a correction formula for the effect of the magnetic pressure on the surface oscillation frequency was developed [15] allowing the faithful evaluation of the surface tension in the presence of strong em-levitation fields as present in ground based em- levitation [16].

The evaluation of the viscosity as an intrinsic material property requires the absence of turbulent fluid flow and other nonlinear fluid flow effects. Under earth gravity (1-g) conditions the electromagnetic forces required to balance the drop weight against gravity are so large that there will always be turbulent fluid flow. As such, turbulence free conditions can only be realized under reduced gravity (μ-g). In addition to the absence of turbulence, the reduced magnetic force on the sample results in a spherical equilibrium shape such that the surface oscillates at a single frequency. In the framework of a programme for thermophysical property measurements in the liquid phase of

a large variety of metals and alloys with liquidus temperatures ranging from 1073 to 2130 K an eml processing device was installed on the International Space Station (ISS-EML).

In order for the oscillating drop method to result in accurate viscosity values as an intrinsic material property, the parameter range to be applied in these measurements needs to be properly considered. Besides the absence of turbulence which may arise from residual heating this concerns the degree of sample shape deformation which can be applied in the measurement. In that context pronounced non-linear fluid flow effects on the damping time constant of surface oscillations and, thus, on the viscosity evaluated with the Lamb formula have been predicted in a variety of magnetohydrodynamic fluid flow simulations. Because of the lack of suitable reference measurements by standard methods such as the oscillating or rotating cup for many alloys of technological and scientific interest, constraints on experimental parameters derived from numerical modelling and their experimental verification are important for the application of the oscillating drop method for accurate viscosity measurements. In all model calculations known to us the non-linear contributions to the damping result in an increase of the damping time constant relative to that obtained with the Lamb formula for the same viscosity. Conversely, the application of a damping time constant measured under such conditions in the Lamb formula would result in an increased viscosity over that representing the intrinsic material property.

In that context the ISS – EML was used for an investigation of the effect of the initial sample shape deformation on the damping time constant of the surface oscillations in the oscillating drop method. To this end it was first necessary to inspect the surface oscillation signals as a function of time following pulse excitation in order to extract a reliable damping time constant from the experiments. Often that signal exhibited a modulation which in some cases could mimic non-linear effects in the surface oscillation decay. The experiments were performed with the Ni-based superalloys MC2 and LEK94.

In the following we describe some of the theoretical background and motivation of this effort followed by a short description of the experimental set up of the ISS -EML. Then the evaluation of the surface oscillation damping time constant from signals exhibiting various degrees of modulation is considered in more detail, including the possible dependence of the damping time constant on the initial deformation. In the discussion we focus on the model of Etay et al. [17] mainly because the authors provide data from which a numerical relation between sample deformation and a correction to the ideal Lamb damping can be derived which can be tested experimentally. As compared to previous parabolic flights, the experiments on the ISS provided a much better signal quality over a larger temperature range allowing to test for the presence of non-linear effects which previously was not possible.

2 GENERAL CONSIDERATIONS

In the oscillating drop method as performed in an eml device under reduced gravity conditions a sample is heated into the liquid phase by a radio-frequency (rf-) em-field. After having reached a preset maximum temperature the heating field is turned off. In the following nearly force free cooling phase short pulses of the em-field are applied for the excitation of surface oscillations. The surface oscillations are recorded, see below, and the damping time constant is evaluated.

The dynamics of an oscillating levitated liquid droplet with or without the presence of an electromagnetic field has received considerable attention from the modelling and experimental side [18–22]. In part this is owed to the importance of non-contact em- processing of reactive liquid metallic alloys in industrial casting such as cold crucible or induction skull melting. An other aspect is to test and improve the numerical modelling [18, 23] of magnetohydrodynamic phenomena [24–26] including shape deformations of an em-levitated droplet and surface oscillations, turbulent fluid flow and non-linear fluid flow phenomena [27, 28]. A considerable amount of modelling work was concerned with thermophysical property measurements on electromagnetically levitated droplets in particular of the viscosity and surface tension by the oscillating drop method. Berry et al. [29] modelled the oscillations of a liquid droplet in an electromagnetic levitation device under conditions very close to the experiments to be described below. They find that the fluid flow in the droplet after the end of the surface oscillation excitation pulse is dominated by turbulence resulting in large deviations of the calculated damping time from that obtained with the Lamb formula for the same viscosity. With that observation they explain some unusually large viscosities measured in some microgravity experiments. The question arises how long these turbulent fluid flows persist. Bojarevics and Pericleous [30, 31] in principle come to a similar conclusion. Using parameters such as sample diameter, viscosity and electrical conductivity close to the current experiments they obtain that the initial turbulence following the excitation pulse is damped out after a time of < 0.3 sec. A similar result was obtained by Etay et. al. [17]. In the context of the current experiments Etay et al. [17] modelled the effect of the non-linear term in the Navier-Stokes equation on the observed damping time. They define a Reynolds number:

$$\mathrm{Re}_{\mathrm{nl}} = R_{\mathrm{o}}\,\varepsilon_{\mathrm{o}}\,2\pi\nu_{\mathrm{sc}}\,\frac{R_{\mathrm{o}}}{h} \tag{3}$$

with R_{o} the equilibrium sample radius, $R_{\mathrm{o}}\varepsilon_{\mathrm{o}}$ the initial sample deformation along the field-direction and $h = \eta/\rho$ the kinematic viscosity with η and ρ the dynamic viscosity and density, respectively. ν_{sc} is the surface oscillation frequency and $R_{\mathrm{o}}\varepsilon_{\mathrm{o}}\,2\pi\nu_{\mathrm{sc}}$ is the initial surface velocity in the direction of the

maximum sample shape deformation. For $Re_{nl} > 5$ they find an increasing deviation between the damping time constant observed in their modelling, the 'measured' damping time constant, k_E, and that predicted by the Lamb formula, k_L, for the same viscosity. The relative deviation between k_E and k_L is expressed by a correction term Δk_E such that the measured damping constant is given by:

$$k_E = k_L(1+\Delta k_E) \tag{4}$$

Δk_E is a strong function of Re_{nl} i. e. of $R_o\varepsilon_o$ and η. With the temperature coefficient of the surface tension in the order of 4×10^{-4} $Nm^{-1}K^{-1}$ its effect on Re_{nl} as a function of temperature can be neglected. The same holds for the density. In the model of Etay et al. $\Delta k_E(Re_{nl}) \rightarrow 1$ for $Re_{nl} > 1000$. A qualitatively similar result was obtained in Reference [32], however, the scale of the deviation from the Lamb formula was much larger than that given by Etay et al.

In our previous evaluations of the viscosity from oscillating drop measurements with an eml on board parabolic flights we have set the measured damping time constant $k_m = k_L$ and used that number in the Lamb formula for the evaluation of the viscosity. Most of these measurements were performed in the range of $10 \leq Re_{nl} \leq 500$ which would have resulted in substantial errors of the viscosity such obtained. Moreover, if valid, the results of these model calculations would pose severe restrictions on the allowed sample shape deformation and, thus, on the temperature range available for viscosity measurements for any given alloy.

It should be noted that these modelings are quite complicated and still a matter of current research. For example, in Reference [26] the surface oscillation frequency recovered from the modelling is very different from the value used as an input parameter. Interestingly, Spitans et al. [33] predict a 3 to 5 % lowering of the surface oscillation frequency for large initial sample deformation for very much the same conditions as present in the current ISS experiments. Such a deviation was indeed observed in the analysis of recent experiments with the ISS-EML by Xiao et. al. [34]. As an other example, for $Re_{nl} \approx 25$ Spitans et al. [33] predict a ratio of $k_m/k_L \approx 3$ while in the work of Etay et al. [17] for the same Re_{nl} a value of $k_m/k_L = 1.25$ is obtained. To further complicate matters it has recently been suggested that tangential surface flows could also have an effect on the measured damping time constant [35] in the oscillating drop method.

A comparison of the model predictions with experiment requires reliable data from the experimental side. The surface oscillations are evaluated from an image recording with a high frame rate digital camera corresponding to a two dimensional projection of the oscillating droplet. The frame rate is typically a factor of 3.5 to 10 higher than the surface oscillation frequency. The surface oscillations can be described by the spherical harmonic functions $Y_{2m}(t) = sin(2\pi\nu_{sc}t)\ Y_{2m}(\theta,\varphi)$ of order 2 with $m = 0, \pm1, \pm2$ which do not exhibit

spherical symmetry. As a consequence, the shape of the two dimensional projection recorded with the cameras will in general depend on the position of the camera [36]. Vice versa, if the sample rotates around an axis with an arbitrary direction relative to the optical axis of the recording system the two dimensional projection will, in addition to the shape variation originating from the surface oscillations, exhibit a shape variation originating from the rotation and, in general, precession and nutation which will add further complexity to the time variation of the projected image. Such effects are not particular to electromagnetic processing or microgravity conditions but will also be present in other ground based levitation techniques [37]. The resulting modulation of the recorded surface oscillation decay makes the evaluation of the damping time constant difficult. Moreover, signal shapes can result which, if taken at face value, could mimic the presence of non-linear contributions to the damping. Such effects will be investigated in section 4.

The effect of rotation and precession on the surface oscillation spectrum under force free conditions was investigated by several authors [38] regarding the question of how to recover the undisturbed Rayleigh oscillation frequency from the in part complex surface oscillation spectra [39]. It was found that rotation and precession resulted in symmetrically split oscillation spectra and that the undisturbed surface oscillation frequency corresponded to the arithmetic average of the different frequency maxima of the oscillation spectrum.

3 EXPERIMENTAL ELEMENTS

The experiments were performed with the eml device, ISS – EML, on the international space station. The principal set up is very similar to the eml-device installed on board a parabolic flight airplane and has been described in detail elsewhere [40]. In short: The core of the ISS-EML are the UHV compatible stainless steel sample and process chambers. Both are connected to a vacuum and to a gas circulation system. Operation can be under high vacuum at a pressure in the range of $1. \times 10^{-7}$ mbar or under flowing or static He or Ar gas. The gas circulation system is equipped with a gas cleaning unit providing a nominal O_2 and H_2O purity ≤ 1 ppb. Samples are contained in a sample holder with either a cup or an open cage structure. The experiments reported here were performed with cage sample holders. For processing, a sample holder is transferred from the sample into the process chamber into the center of an induction coil providing a combination of a rf-quadrupole and rf-dipole induction field for positioning and heating, respectively. The sample chamber is equipped with UHV compatible windows for sample observation and temperature measurement and with feedthroughs for the rf-power to the position and heating coil system. The sample temperature is measured in the polar position along the symmetry axis of the dipole heating field by a pyrometer with a 100 Hz sampling rate. The pyrometer is integrated in a digital, axial,

camera operating with maximum frame rate of 150 Hz. A second camera, radial camera, is positioned in a perpendicular direction viewing in the equatorial plane of the sample in the center of the coil system. For measurement of the surface tension and viscosity the radial camera is operated with a frame rate of 400 Hz.

A typical temperature-time profile of the application of the oscillating drop method is shown in Figure 1. The sample was the Ni-based superalloy MC2 with a diameter of 6.52 ± 0.02 mm. Starting in the solid phase the sample is heated, melted and heated further in the liquid phase. After having reached a preset maximum temperature the rf-heating field is turned off. In the nearly force free cooling phase pulses of the heating field are applied for the excitation of surface oscillations. The first excitation pulse was applied in the stable liquid phase just above the liquidus temperature, the second in the undercooled liquid phase. The excitation pulse amplitude, duration and shape could be varied. In the current investigation the pulse shape was throughout rectangular with a duration of 0.10 s and the amplitude was varied. The vertical arrow in the Figure indicates the onset of recalescence in the undercooled liquid phase. The apparent temperature increase near the end of the solidification plateau is caused by a surface roughening upon complete solidification resulting in an increase of the emissivity. The reverse is observed during melting.

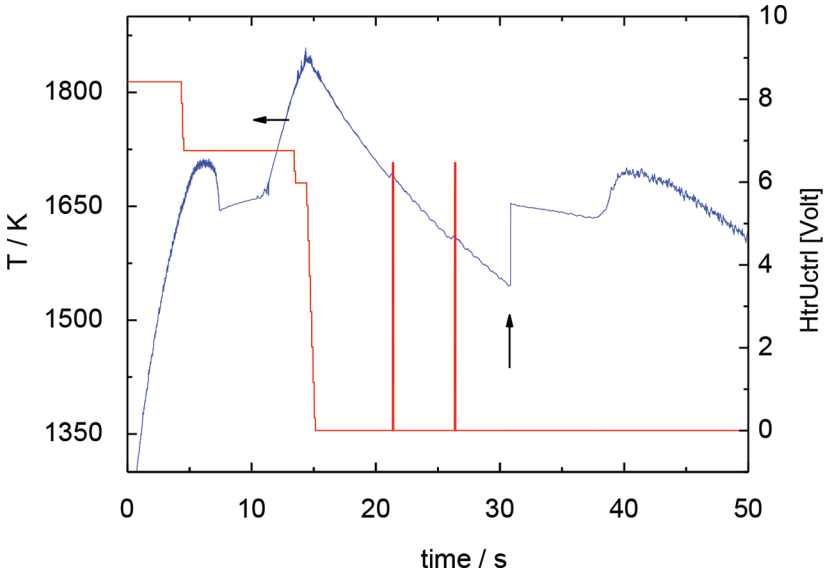

FIGURE.1
MC2, Cycle06. Temperature-time profile of processing an MC2 alloy for application of the oscillating drop method with the ISS-EML. Temperature indicated by an arrow is shown on the left hand the rf-heater control voltage on the right hand ordinate. The vertical arrow indicates recalescence and solidification.

During the free cooling phase the em-positioner power was reduced to a minmum acceptable value to guarantee stable positioning of the liquid sample. It was verified that under this conditions and in the parameter range of the experiments regarding the electrical resisitivity, sample diameter and viscosity the positioner field does not induce turbulent fluid flow [41].

The sample deformation as a function of time is evaluated from the digital image recording by using a dedicated software [42]. The image analysis software provides several measures of sample shape deformation such as the sample radii in two perpendicular directions, their sum and difference, the variation of the total projected area and the difference area between the latter and a circle with the radius of the undisturbed sphere. In the standard analysis coordinates system, the Y-axis is directed along the dipole field axis and the X-axis perpendicular to it. The analysis coordinate system can be rotated by a variable angle. The fitting of the sample circumference provides a sub pixel resolution which allows to analyze sample shape deformations ≥ 0.5 %.

The data acquisition system provides a synchronization between temperature-time data from the pyrometer and the frame numbers of the axial and radial camera files. From that a unique correlation between time – temperature – measure of sample shape deformation is obtained. In practical terms these properties are listed as columns in a data file allowing a straightforward mapping of properties calculated as a function of temperature on the time axis.

The maximum force of an em-pulse acts perpendicular to the axial direction in the equatorial plane of the sample directed towards the sample center. Thus, the maximum initial deformation of the liquid sample following an excitation pulse is along the Y-axis in the radial camera view. In the following listed values of the initial sample shape deformation always refer to the deformation along the Y-axis in the radial camera view.

4 MODELLING OF SURFACE OSCILLATIONS

The difficulty of extracting reliable surface oscillation decay time constants is demonstrated in Figure 2 showing the variation of the X-radius of the sample as a function of time following the two surface oscillation excitation pulses shown in the temperature-time profile of Figure 1. The experiment was performed with the Ni-based superalloy MC2 with a liquidus temperature of 1663 K. The signal shown was high pass filtered with a lower frequency limit of 15 Hz compared to an average surface oscillation frequency of 35 Hz. This is a typical example of the kind of surface oscillation signals obtained in the ISS-EML or in parabolic flight experiments. The two pulses were applied at $t = 5.5$ and at $t = 10.5$ s. The variation of the radius in the time interval between $0 < t < 5.5$ s was caused by the surface oscillations following turning off of the rf-heater generator control voltage after the sample temperature had

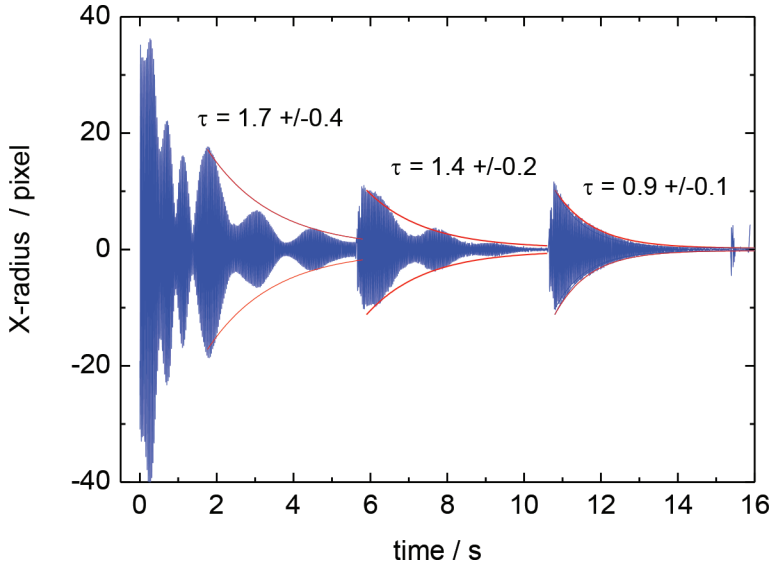

FIGURE 2
MC2, Cycle 06. Variation of X-radius as a function of time evaluated from the radial camera digital image recording of the sample shape during the temperature-time profile shown in Figure 1. High pass filtered signal.

reached a preset maximum value. The temperature range covered by the radius variation shown in Figure 2 was from $T = 1853$ to 1544 K. Also shown in the Figure are exponential fits to the maxima of the modulated signals following turning off of the rf-heater and of the first excitation pulse and an exponential envelope fit to the surface oscillation maxima following the second excitation pulse. Surface oscillation decay times obtained in this way from different cycles were used for the calculation of starting values of the viscosity as a function of temperature and a first evaluation of the Arrhenius parameters, see below. In the above example the initial sample shape deformation following the excitation pulses was 20 ± 2 pixels corresponding to a 10% initial radius deformation.

The radius variations following the initial turning off of the rf-heating generator voltage and the first excitation pulse clearly exhibit a modulation. The first one appears to consist of more than one frequency while the second one appears to be single frequency. The frequency of the surface oscillations is obtained from a fast Fourier transform (FFT) of selected time slices of the radius variation. The FFT spectrum of the time slice between $t = 5.5$ and 10.5 s shows a central peak corresponding to the undisturbed surface oscillation frequency and two sidebands with a symmetric splitting of $\pm$ 0.66 Hz.

In general, the shape of the radius variation as a function of time is determined by:

i) the surface oscillation frequency as the 'carrier' frequency
ii) the damping of the surface oscillations
iii) the modulation frequency and its phase relative to the surface oscillation excitation pulse
iv) the modulation depth, r_{mod}

For a single modulation component this can be modelled by the following function:

$$\begin{aligned} R(t) = \{A_o + A_1 \sin[2\pi\nu_{mod}(t-t_o)+\varphi_{mod}]\}\times \\ \sin\{[2\pi(\nu_{SC}+\gamma_{SC}(t-t_o)](t-t_o)+\varphi_{SC}\}\times\exp[-k_m(t-t_o)]+ \\ B_o \sin[2\pi\nu_{SC}(t-t_o)+\varphi_b] \end{aligned} \quad (5)$$

A_o, A_1: amplitudes of the surface oscillations and of the modulation, respectively.
ν_{sc}, ν_{mod}: frequency of the surface oscillations and of the modulation, respectively
φ_{sc}, φ_{mod}: phases of the surface oscillations and of the modulation at starting time t_o
t, t_o: running time and starting time, respectively
γ_{sc}: temperature coefficient of the surface oscillations
k_m: surface oscillation damping time constant
B_o: remaining sinusoidal baseline signal

$$r_{mod} = \frac{A_1}{A_o + A_1}$$

Values for A_o, $A_{1,}$ φ_{mod}, φ_{sc}, t_o and B_o can be obtained from inspection of the time signal. ν_{mod}, ν_{sc} can be obtained from the FFT of suitable time slices. The simulation includes a time-temperature dependent surface oscillation frequency with temperature coefficient γ_{sc}. This is not the temperature coefficient of the surface tension itself as $\nu \propto \sigma^{1/2}$. The temperature coefficient is in the order of a few 10^{-4} s^{-1} K^{-1}. The surface tension is calculated according to the Rayleigh formula Eq. (2) with the temperature dependence given by

$$\sigma(T) = \sigma_o - \gamma_{st}(T - T_o) \quad (6)$$

For the particular example of MC2 in Cycle 06 we obtain with T in K

$$\sigma(T) = 1.67 - 1.48\times10^{-4}(T - 1663) \quad Nm^{-1} \quad (7)$$

which is in the range of values for other Ni-based superalloys [43, 44].

The damping time constant of the surface oscillations is obtained as follows. First it is evaluated at selected temperatures from more rough and ready

exponential envelope fits as shown in Figure 2. From these the viscosity, η, is calculated according to the Lamb formula. Values such obtained are plotted in an Arrhenius representation of the viscosity according to:

$$\ln \eta \;=\; \ln \eta_{\mathrm{o}} + \frac{\Delta E_{\mathrm{a}}}{k_{\mathrm{B}}}\,\frac{1}{T} \tag{8}$$

From a linear fit of $\ln(\eta)$ as a function of $1/T$ the prefactor η_{o} and the activation energy ΔE_{a} are obtained. With these data $k_{\mathrm{L}}(T)$ is obtained as a continuous function of T according to:

$$k_{\mathrm{L}}(T) \;= \frac{20\pi}{3}\,\frac{R_{\mathrm{o}}}{M}\,\eta_{\mathrm{o}} \exp\!\left(\frac{\Delta E_{\mathrm{a}}}{k_{\mathrm{B}} T}\right) \tag{9}$$

and is then inserted into Eq. (5) with $k_{\mathrm{m}} = k_{\mathrm{L}}$. The procedure is now to further refine η_{o} and ΔE_{a} by fitting of Eq. (5) to surface oscillation decays which extend over a larger temperature range and preferably do not exhibit modulation. The final values of η_{o} and ΔE_{a} should then provide a good representation of all measures of surface deformation as a function of time - temperature which can be described by Eq. (5).

If in addition to the pure Lamb damping non-linear effects depending on the sample deformation are present, k_{L} in Eq. (5) must be replaced by k_{E} as given in Eq. (4). In reference [17] Etay at al. provide numbers of Δk_{E} as a function of Re_{nl} which are reproduced in Figure 3 together with a sigmoidal fit. The sigmoidal fit represents $\Delta k_{\mathrm{E}}(R_{\mathrm{nl}})$ quite well allowing to represent $\Delta k_{\mathrm{E}}(R_{\mathrm{nl}})$ as a continuous function of the Arrhenius parameters of the viscosity and the sample shape deformation. This can then be inserted into Eqs. (4) and (5) allowing to fit a measured surface oscillation decay signal as a function of η_{o} and ΔE_{a} and $R_{\mathrm{o}}\varepsilon_{\mathrm{o}}(T)$. The latter can be obtained as a continuous function from an envelope fit to a measured surface oscillation decay leaving, in the absence of modulation, η_{o} and ΔE_{a} as free parameters for an envelope fit.

5 SPECIFIC APPLICATIONS

5.1 Exponential envelope fits

In Figure 4 the variation of the Y-radius following the second surface oscillation pulse in Cycle 03 is shown. This pulse was chosen as a starting point of the analysis because it covered a temperature range from 1718 to 1585 K without any apparent modulation. The insert in the Figure shows the end of the pulse in more detail.

The upper curve labelled ‘Lamb’ represents an envelope fit calculated with Eq. (5) with the fast surface oscillation term omitted and with a temperature-time

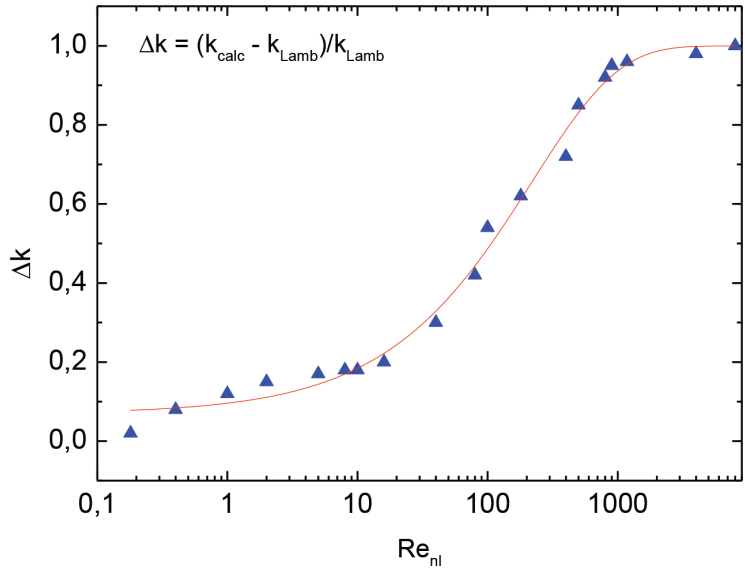

FIGURE 3
Δk_E as a function of R_{nl} as given in Ref. [34]. Full line sigmoidal fit of $\Delta k_E(R_{nl})$.

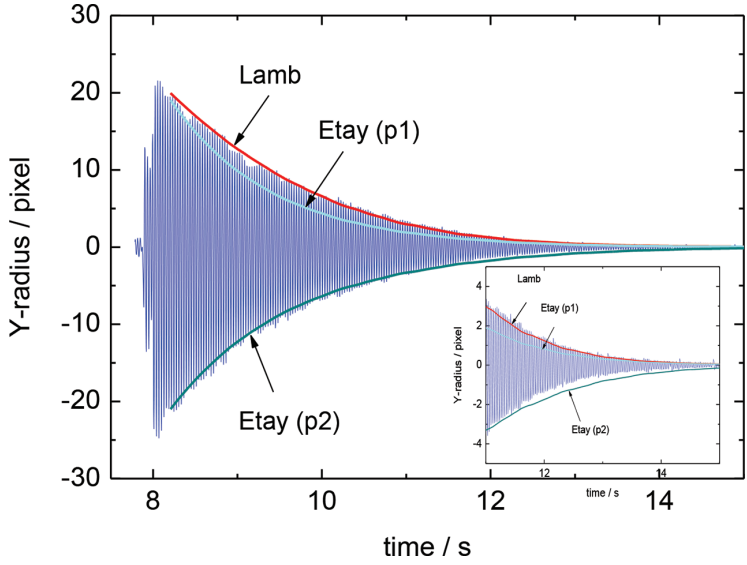

FIGURE 4
MC2, Cycle 03. Y-radius variation as a function of time following the second excitation pulse superimposed with envelope fits according to the Lamb, red curve, and Etay, light blue and cyan curves, damping model. The insert shows the low amplitude part of the surface oscillation at longer times in more detail. For details see text.

dependent k_L(T) according to Eq. (9). Starting values for ΔE_a and η_o were obtained as described above. The values of ΔE_a and η_o such obtained were used throughout for the calculation of $k_L(T)$ for the MC2 alloy unless otherwise stated. A very good match between the measured and calculated variation of the surface ocillation amplitude as a function of time is obtained. The success of this approach depended on the very good data quality available in the ISS experiments. A similar perfect match between the measured amplitude variation and a calculated envelope function with different values of η_o and ΔE_a was obtained in Cycle 04 of the Ni-based superalloy LEK94 processed in the same experiment series.

The values of ΔE_a and η_o such obtained are not unique. Within error limits quite different combinations of ΔE_a and η_o resulted in similar envelope fits with marginally different viscosities showing that a temperature range of 140 K is too small to unambiguously fix the Arrhenius parameters even for the very good signal quality exhibited here.

The second curve from the top, labelled 'Etay(p1)' was calculated to show how the envelope function would look if the same Arrhenius parameters used for the curve labelled 'Lamb' were applied in the Etay model for the calculation of R_{nl} with $R_o\varepsilon_o(T)$ taken from the 'Lamb' envelope fit and $\Delta k(R_{nl})$ taken from Figure 3. $k_L(T)$ was calculated from Eq. (9) and inserted in Eq. (4) to calculate the Etay type damping time constant, k_E, which was then inserted in Eq. (5) with $k_E = k_m$. As expected a steeper initial decay of the surface oscillations is observed. Both curves converge for a relative shape deformation ≤ 1 %.

The bottom curve labelled 'Etay (p2)' was obtained by using the Etay model with a different set of ΔE_a and η_o values adjusted for the best match with the measured signal for the calculation of the envelope curve. With the exception of the low oscillation amplitude part of the signal for $t > 11.5$ s also the Etay model provided a good representation of the measured amplitude as a function of time. The discrepancy for $t > 11.5$ s is in the range of < 2 pixels and it appears difficult to assign a systematic significance to it.

To further test the validity of the above approach Figure 5 shows the Y-radius variation in Cycle 06 following the first and second excitation pulse with an envelope fit according to Eq. (5) with a Lamb type damping. The pulses covered the temperature range from 1691 to 1548 K extending the temperature range to 173 K for which the pure Lamb type damping, with the same ΔE_a and η_o values for the Arrhenius temperature dependence of the viscosity, provided a very good envelope fit of the measured amplitude variation independent of the degree of sample shape deformation.

5.2 Modulated response

Modulated surface oscillation decays are ubiquitous in these experiments. The shape of the signal can exhibit a considerable degree of variation from obvious to subtle. In some cases, it could appear as indicating a non-linear effect in the damping of surface oscillations. As an example Figure 6 shows

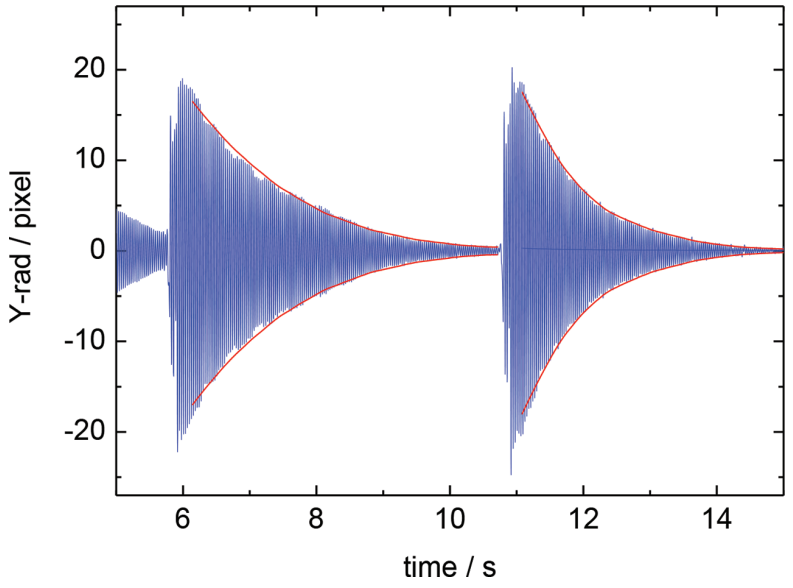

FIGURE 5
MC2, Cycle 06. Variation of the Y-radius as a function of time following the first and second surface oscillation excitation pulse. Also shown are calculated envelope functions representing the variation of the oscillation amplitude as a function of time.

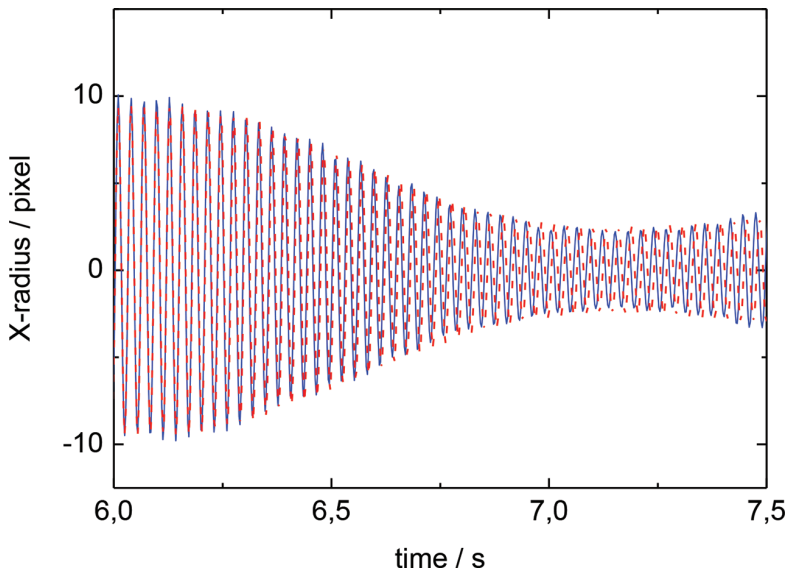

FIGURE 6
MC2, Cycle 06. X-radius as a function of time following the first surface oscillation excitation pulse. Full line, blue, measured signal, dashed line, red, simulated signal.

the X-radius variation following the first excitation pulse in Cycle 06 in more detail superimposed with a simulation according to Eq. (5) with a Lamb type damping. A very good match is observed. The surface oscillation frequency was calculated from a linear fit to the average of the surface tension as a function of temperature evaluated from five cycles. The direct simulation of the surface oscillations provides a very sensitive test of the surface oscillation frequency. The parameters used for the modulation were: $\nu_{mod} = 0.64$ Hz, $\varphi_{mod} = 0.0$ rad, $r_{mod} = 0.29$, $A_o = 9.0$ pixel and $\varphi_{sc} = -0.9$ rad. The most sensitive parameters to achieve good agreement between the measured and simulated signal are ν_{mod}, φ_{mod} and r_{mod}.

In this context it is interesting to demonstrate the effect of a variation of φ_{mod} and r_{mod} on the simulated signal shape. Figure 7 shows a signal calculated with the Lamb damping model and with modulation parameters $\nu_{mod} = 0.25$ Hz, $\varphi_{mod} = 1.5$ rad and $r_{mod} = 0.15$. The temperature range was between $T_1 = 1683$ and $T_2 = 1611$ K. For the first 2 s the envelope shape exhibits a much faster decrease than for $t > 2$ s. If taken at face value such a signal shape could be interpreted to indicate the presence of nonlinear fluid flow effects with an initial fast decay followed by a much smaller decay time constant. Such signal shapes were indeed observed. However, in the simulations presented here, see e.g. in Figure 7, they are the result of a modulation

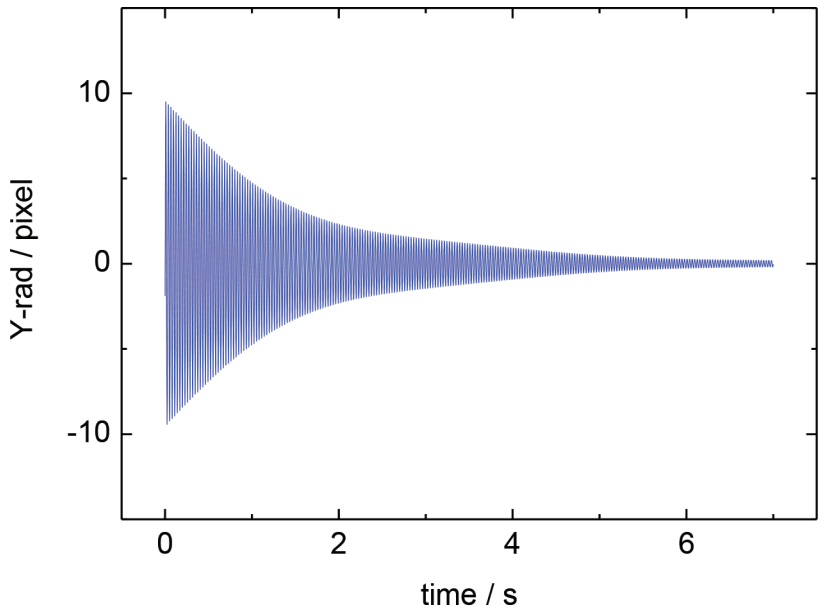

FIGURE 7
MC2. Simulated surface oscillation decay with modulation with Lamb type damping. Same Arrhenius parameters of the viscosity as in previous cycles.

effect on top of a monotonously increasing k_L(T) as a function of decreasing temperature.

With that observation in mind a measured surface oscillation decay from Cycle 09 of the same alloy was analysed which displayed an apparently fast initial decay of the surface oscillations followed by a smaller one. Figure 8 shows the variation of the X-radius as a function of time. Two excitation pulses were applied at temperatures of $T = 1647$ K and $T = 1580$ K covering a temperature range of 100 K all in the undercooled liquid phase. The surface oscillations following the second excitation pulse were stopped by the onset of solidification. The amplitude of the excitation pulses was reduced such that in comparison with the previous cycles only half the force was applied resulting in an initial shape deformation of 6 %.

Regarding the first excitation pulse, shown in the Figure are two sets of envelope curves. The upper one was calculated with the Lamb, the lower one with the Etay damping model using the same respective Arrhenius parameters which resulted in the very good match between the measured and calculated envelopes shown in Figure 4. Both envelope curves do not match the

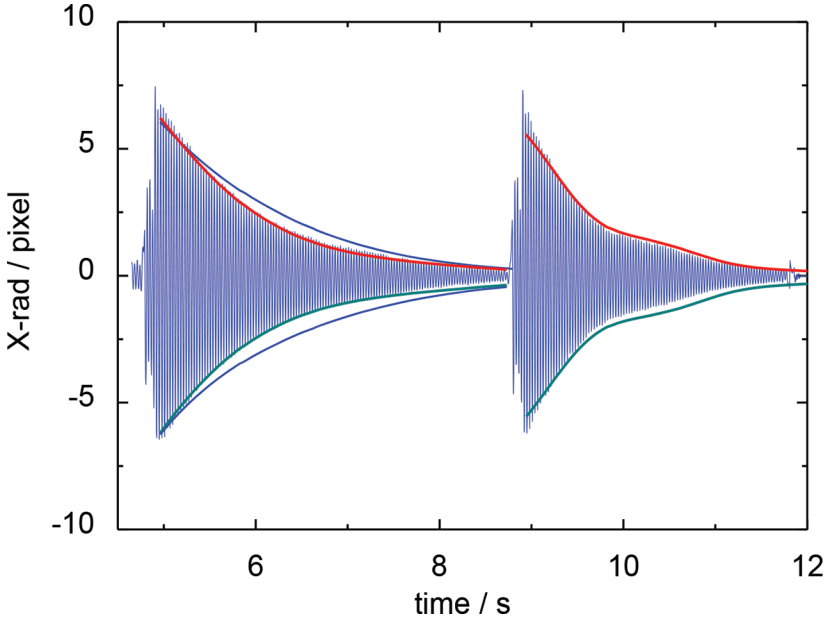

FIGURE 8
MC2, Cycle 09. X-radius as a function of time following two excitation pulses. First pulse from the left. Blue curves: envelopes calculated with the Lamb, top, and Etay, bottom, damping model, no modulation. Red curve: envelope calculated with the Lamb damping model with modulation. Cyan curve: envelope calculated with the Etay damping model with modulation. Second pulse: Red curve: envelope calculated with the Lamb damping model with modulation. Cyan curve: envelope calculated with the Etay damping model with modulation.

measured signal. Considering a modulated response according to Eq. (5) a very good match between the envelopes calculated with the Lamb, upper part, and Etay damping model, lower part, and the measured signal is obtained. The modulation parameters for both simulations were the same with $\nu_{mod} = 0.24$ Hz, $\varphi_{mod} = -5.0$ rad and $r_{mod} = 0.15$. This example demonstrates that a low frequency modulation with a small r_{mod} can mimic a fast initial surface oscillation decay followed by a slower one. For example, an exponential envelope fit with $k_m = const.$ applied to the first 1.5 s of the signal gives $k_m = 1.0$ s^{-1} while the average $k_L(T)$ in that temperature interval is obtained as $k = 0.68$ s^{-1} resulting in viscosities of 17.9 and 12.2 mPa.s, respectively, with obvious consequences for practical viscosity measurements.

The effect of modulation is more obvious in the second pulse. The upper envelope curve was calculated with the Lamb damping model. The modulation parameters were $\nu_{mod} = 0.62$ Hz, $\Delta\varphi_{mod} = 0.2$ rad, $r_{mod} = 0.11$. The match with the measured signal is very good. The lower curve was calculated with the Etay damping model with the same modulation parameters. The match with the measured signal is not as good as it was for the first pulse. The match can be improved with a change of the Arrhenius parameters used for the Etay model but that resulted in a similar mismatch of the envelope in the first pulse. The same holds for the Etay envelope curve shown in Figure 4. A better match at the lower temperatures results in a worse match at the higher ones. A similar observation was made by fitting an envelope function with the Lamb and Etay type damping to a measured surface oscillation signal of the alloy LEK94. As such, if considered together, there appears to be a systematic difference between the quality of the fits obtained with the Lamb and Etay damping independent of the presence of modulation. It must be pointed out, however, that while appearing systematic the differences between the Etay model envelope fits and the measured signal are small.

6 DISCUSSION

In the previous section it was demonstrated that a variety of measured surface oscillation decays exhibiting different signal shapes could be well represented by a simulated signal consisting of the superposition of an undisturbed carrier frequency and a modulated component with the damping according to the Lamb model. With that approach it could be demonstrated that over a temperature range of 220 K, independent of the sample shape deformation, the variation of the surface oscillation amplitude as a function of time-temperature could be well described by a Lamb type damping with the viscosity exhibiting an Arrhenius temperature dependence with a single set of η_o and ΔE_a values. In particular signal shapes such as shown in Figure 7, calculated, and Figure 8, measured, with an apparent initial fast decay of the oscillations

amplitude could be very well represented by the above model. This finding supports the conclusion that signal shapes like that following e.g. the second excitation pulse shown in Figure 8 can not by themselves be taken as evidence for the presence of non-linear contributions to the damping. This statement holds irregardly if the Lamb or Etay damping model was applied for the calculation of envelope functions.

In the following we focus on the model presented by Etay et. al. [17] because these authors provided explicit values of the non-linear correction to the Lamb damping which could be used for a comparison with experiment. As shown above in Figures 4 and 8, the mathematical representation of this model when used with a different set of Arrhenius parameters also provided a good representation of the measured surface oscillation signals as a function of time - temperature. The differences between the envelope functions calculated by the Lamb and Etay damping model and the measured signal appear to be systematic but are too small to allow an unambiguous differentiation between the two damping models. Due to the nature of the non-linear models their damping time constant is always larger than that of pure Lamb damping for the same vicosity. The viscosities corresponding to the Lamb and Etay(p2) envelope curves shown in Figure 4 are shown in Figure 9 demonstrating that the Lamb and Etay models result in significantly different vis-

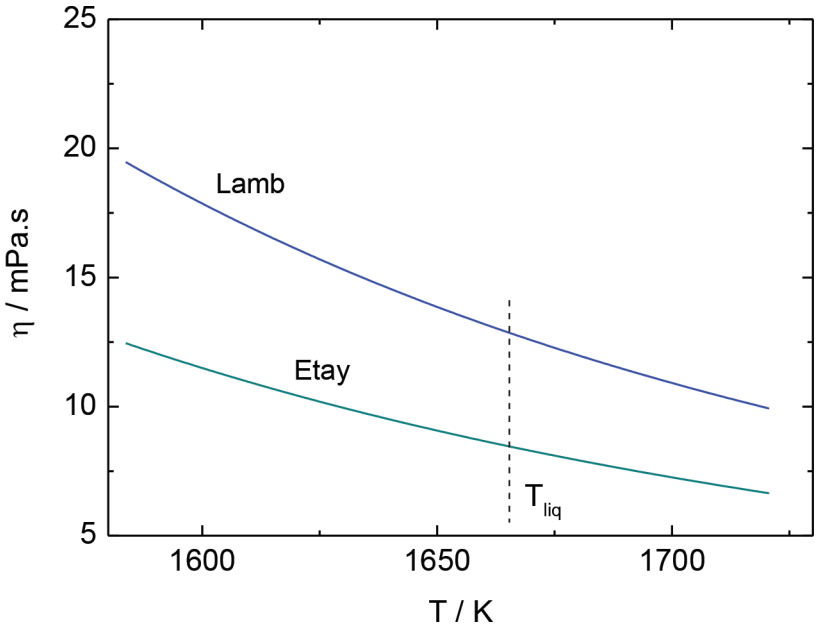

FIGURE 9
MC2, Cycle 03. Viscosity as a function of temperature corresponding to the Lamb and Etay(p2) envelope fits shown in Figure 4.

cosities evaluated from the same measured surface oscillation decay. The same conclusion is obtained from the analysis of the modulated surface oscillation decays shown in Figure 9. The small amplitude, high viscosity part of the measured signal decay is better represented by the pure Lamb damping. Again it appears difficult to assign a systematic significance to that observation because of the absolute small signal level of approx. two pixels and less.

Considering the different mathematical representations of the damping in the Lamb and Etay models the similarity of the Lamb and Etay(p2) envelope fits in Figure 4 appears astonishing. Indeed, it was first thought that the perfect match of the Lamb envelope fit with the measured variation of the oscillation amplitude as a function of time-temperature would be a sufficient criterion to conclude the absence of non-linear fluid flow effects in the damping of surface oscillations. With the data shown this far this is not the case. The similarity of both envelope fits is obtained in that the lower Lamb contribution to the viscosity in the Etay model, see Eq. (4), is balanced against the higher viscosity in the Lamb fit by the steep combined temperature and amplitude dependence of $\Delta k_E(R_{nl})$ resulting in quite similar damping time constants in both models, at least in the parameter range available in this investigation. For visualization, Figure 10 shows Re_{nl} and Δk_E as a function of time used for the calculation of the envelope fit with the Etay damping model shown in Figure 5.

As a consequence, we are left with a situation where envelope fits or direct simulations of the surface oscillation signal do not allow to unambiguously

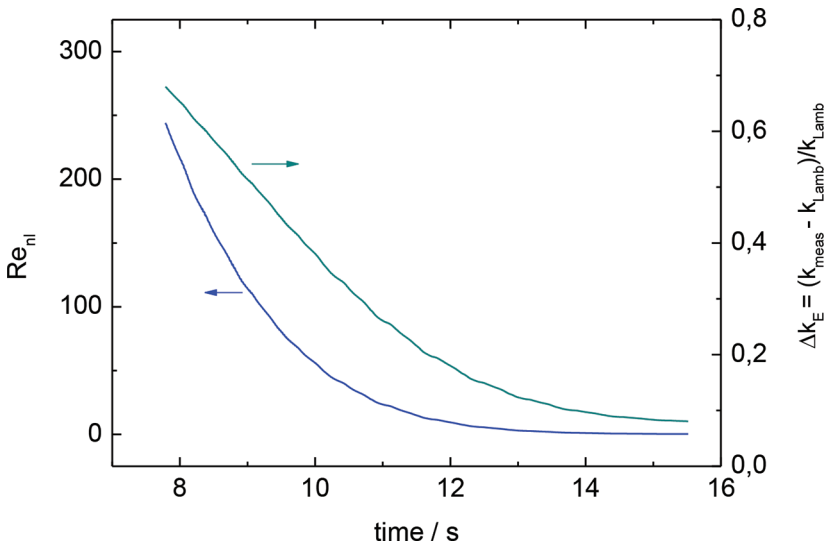

FIGURE 10
MC2, Cycle 03: Re_{nl} shown on the left hand ordinate and Δk_E shown on the right hand ordinate as a function of time for the second surface oscillation pulse shown in Figure 6.

differentiate between the two models with the obvious difficulty of assigning physically correct values of the viscosity to the alloy at hand. For the Ni-based superalloys comparison with viscosity values obtained by the oscillating cup method are available for alloys of similar composition [45, 46, 47, 48]. Values of the viscosity at the liquidus temperature are the range of 6.8 to 8.2 mPa.s. For MC2 these would favor the result obtained with the Etay model, i. e.$\eta(T_{\mathrm{liq}}) = 8.6$ mPa.s, as compared to that obtained with pure Lamb damping which gave $\eta(T_{\mathrm{liq}}) = 12.8$ mPa.s. Applying the same analysis to the alloy LEK94 we obtain $\eta(T_{\mathrm{liq}}) = 5.6$ mPa.s for the Etay type damping and $\eta(T_{\mathrm{liq}}) = 7.4$ mPa.s for the pure Lamb damping. The latter value is well in the range of accepted values for the Ni-based superalloys while the former is not. As mentioned above there may be other effects [35] such as tangential surface flows which could contribute to high measured damping time constants in the oscillating drop method. Such effects have not yet been experimentally investigated.

In order to further elaborate the issue, the scaling of k_{m} measured at the same temperature but with a different degree of sample shape deformation is considered. To that end surface oscillation decays obtained in different cycles which a) did not exhibit an apparent modulation and b) where one signal had decayed to low amplitudes, < 6 pixels, and the other was at its maximum amplitude between 20 and 14 pixels in the same temperature range, were considered. k_{m} was obtained by a simple exponential decay fit to the variation of the oscillation amplitude as a function of time in a time interval of ± 0.7 s around the measurement point. The ratio of the damping time constants such obtained is compared to that calculated with the Etay model which gave the good fit to the signal envelope shown for example in Figure 4. Results are listed in Table 1. The fist column lists the alloy and the cycle numbers used for the comparison with the first number indicating the cycle where the oscillation amplitude was large and the second the cycle where the oscillation amplitude was smaller. In the column $Re_{\mathrm{E}}(1)/Re_{\mathrm{E}}(2)$ the corresponding *Re*

TABLE 1
Ratio of surface oscillation damping time constants measured and calculated with the Etay damping model for the same temperature but with different sample shape deformations listed in columns column k_m-ratio and column k_E-ratio, respectively. Column, *Re*(1)/*Re*(2), lists the Etay model *Re* numbers evaluated for the cycles with the large and small sample shape deformation. Column, Alloy/Cycles, lists the alloy and cycle numbers. The first number refers to the cycle with the higher oscillation amplitude.

Alloy/Cycles	T_{av}/K	Re(1)/Re(2)	k_E-ratio	k_m-ratio
MC2/06/03	1603	136/1	1.26	1.01
MC2/13/12	1653	135/22	1.23	1.03
LEK94/04/02	1618	226/41	1.28	0.98
LEK94/ 05/04	1578	195/67	1.23	0.94

numbers calculated with the Etay damping model are listed. The column k_E-ratio lists the ratio of the damping time constants calculated with the Etay model and the column k_m-ratio lists the ratio of the measured damping time constants obtained in the two cycles listed in the first column. As a first result, the average value of the k_m-ratio is obtained as 0.99 ± 0.05 indicating that for the same viscosity and in a viscosity range of 8 to 15 mPa.s the k_m-ratio is independent of the degree sample shape deformation. This is not expected from the non-linear damping models. Second, there is a systematic difference beyond error limit between the k_E- and the k_m-ratios showing that for the same viscosity the measured damping time constants do not follow the scaling as a function of Re_{nl} predicted by the Etay model. Other model calculations available in the literature predict an even larger dependence of k_m on the sample deformation for a similar range of sample shape deformation [33]. As such, it is concluded that in the parameter range covered in this investigation non-linear contributions to the damping time constant are absent or at least smaller than that predicted by published results of numerical fluid flow simulations.

The conclusion presented here was obtained in a viscosity range between 8 and 15 mPa.s when evaluated with the Lamb model and for $Re_{nl} < 230$. Increasing the parameter range to larger Re_{nl} numbers could provide more stringent tests of non-linear contributions to the damping of surface oscillations. In the current investigation the latter was limited by the availability of suitable signals at higher temperatures i.e. lower viscosities and temperature constraints regarding the evaporation of sample material.

If the conclusion arrived here is correct it will allow measurements of the viscosity of metallic liquids by the oscillating drop method over a large temperature range unrestricted by a stringent limit for sample deformations $\leq 10\%$. This is easy to realize and will provide good signal to noise ratios in the optical data analysis.

The applicability of that approach depended on i) the availability of reasonable surface oscillation decay times over a large temperature range such as shown in Figure 4 from which the viscosity as a function of temperature could be calculated and Arrhenius parameters of its temperature dependence could be evaluated, ii) of an unmodulated surface oscillation response which could be used for further refinement of the Arrhenius parameters and iii) on the availability of surface oscillation decay signals with a very good signal to noise ratio over a temperature range of about 100 K.

7 SUMMARY

Results of an experimental investigation of the effect of non-linear contributions to the damping time constant of surface oscillations in the oscillating drop method were presented with focus on the effect initial sample shape

deformation. The investigation was performed with an electromagnetic levitation device on board the International Space Station, ISS-EML, with the two Ni-based superalloys MC2 and LEK94 in the context of a programme for thermophysical property measurement of metallic alloys with emphasis on industrial alloys.

As a preliminary, the effect of modulation on the measured surface oscillation decay signal was investigated. Over a temperature range of 220 K many of the observed signal shapes could be well represented by a modulated response with a temperature dependent damping time constant derived from the Lamb formula with a single set of Arrhenius parameters for the temperature dependence of the viscosity, independent of the degree of sample shape deformation. The success of this approach depended on the availability of a few unmodulated surface oscillation decays of very good signal quality. For an initial sample shape deformation $\leq 10\%$, the perfect match of envelope functions calculated with a Lamb type damping and an Arrhenius type temperature dependence of the viscosity with the measured variation of the oscillation amplitude as a function of time - temperature is considered as an indication of the absence or smallness of non-linear contributions to the damping of surface oscillations.

It could be demostrated that a large variety of measured surface oscillation decays could be well represented by a modulated signal with the same Lamb type damping and the same Arrhenius parameters for the viscosity as a function of temperature. In particular, measured signal shapes with a fast initial decay followed by a slower one could be simulated in this way demonstrating that such signal shapes by itself can not be taken as evidence for a non-linear contribution to the damping of surface oscillations. For an initial sample shape deformation $\leq 10\%$ and viscosities in the range from 7.4 to 15 mPa.s this conclusion is independent of the degree of sample shape deformation.

The Etay damping model was also applied for the calculation of envelope functions of measured surface oscillation decays. With a different set of Arrhenius parameters also a good match between the measured and calculated surafce oscillation decay could be obtained. The match was not as good as that obtained with the pure Lamb damping. However, the difference was too small as to base a final conclusion regarding the presence of non-linear contributions on this comparison alone.

Further analysis was based on a comparison of damping time constants measured at the same temperature for different different degrees of sample shape deformation and the corresponding scaling of damping time constants calculated with the Etay model. With a confidence level of about 6% and sample shape deformations in the range from 1 to 10% the measured ratio was independent of the sample shape deformation. This is not expected from non-linear damping models. Moreover, the measured ratios were all in a range of 1.00 ± 0.06 while the ratios prediced from the Etay model were in the range of

1.25 ± 0.03. The range of Re_{nl} numbers tested was between 1 and 226. As a result, there is a distinct difference between the the scaling of the damping time constant as a function of Re_{nl} predicted by the Etay model and the measured one. The numbers obtained here put a limit on the validity of predictions of numerical modelling of the damping of surface oscillations of a liquid droplet.

We are aware that our result is at variance with the predictions from fluid dynamic calculations [17, 26, 29, 34]. As such, it appears necessary to extend the current investigation to larger sample shape deformations and lower viscosities and to comparison measurements performed with other levitation techniques as well and, where it is possible, with established results from classical methods. Such comparisons would be very important for practical viscosity measuements on high temperature reactive alloys.

Finally, it is pointed out that the investigation presented here would not have been possible with parabolic flight experiments due to the limited microgravity time in the liquid phase available in a single parabola, the limited number of parabolas as compared to the number of process cycles available in the ISS experiments and because of the much better micro-g quality on the ISS as compared to parabolic flights.

ACKNOWLEDGEMENTS

The continued support by the DLR Space Administration under contracts 50WM1170 and 50WM1759, W. Dreier, and by the European Space Agency's MAP programme under contract No. 4200014306 /NL/SH, Drs. O. Minster and W. Sillekens, is gratefully acknowledged. Special thanks to DLR German Aerospace Center, Microgravity User Support Center and DLR Institut für Materialphysik im Weltraum, Drs. M. Engelhardt, S. Schneider and J. Schmitz, for their excellent support in preparation and running the experiments and to the facility developer Airbus DS in Friedrichshafen, Dr. W Soellner, Germany.

REFERENCES

[1] Pericleous. K., Bojarevics, V., Djambazov, G., Harding, R. A., Wickins, M., Appl. Math. Modelling, **30** (2006), 1262, http://dx.doi.org/10.1016/j.apm.2006.03.003.
[2] Ludwig,A.,*Int.J.Thermophys.*,**23**(2002),113,http://dx.doi.org/10.1023/A:1019827900959.
[3] Lan, S., Blodgett, M. Kelton, K. F., Ma, J. L., Fan, J., Wang, X.-L., *Appl. Phys. Lett.*, **108** (2016), 211907; https://doi: 10.1063/1.4952724.
[4] Herlach, D., Cochrane, R., Egry, I., Fecht, H.-J., Greer, A. L., *Int. Mat. Rev.,* **38** (1993), 273, http://dx.doi.org/10.1179/095066093790326267.
[5] Wunderlich, R. K., Fecht, H.-J., *Mater. Trans. JIM*, **42** (2001), 565, http://dx.doi.org/10.2320/matertrans.42.565.
[6] Rhim, W.-K., Ohsaka, K., Paradis, P.-F, Spjut, R. E., *Rev. Sci. Instr.*, **70** (1999), 2796, http://dx.doi.org/10.1063/1.1149797.

[7] Paradis, P. F., Ishikawa, T., Yoda, S., *Int J. Thermophys*., **23** (2002), 825, https://doi.org/10.1023/A:1015459222027.
[8] Egry, I., Lohöfer, G., Seyhan, S., Schneider, S., Feuerbacher, B., *Int. J. Thermophys*., **20** (1999), 1005, http://dx.doi.org/10.1023/A:1022686316437.
[9] Egry, I., Diefenbach, A., Dreier, W., Piller, J. *Int. J. Thermophys*., **22** (2001), 569, https://doi.org/10.1023/A:1010753805462.
[10] Wunderlich, R. K., Fecht, H.-J. *Int. J. Mater. Res*., **102** (2011) 1164, https://doi.org/10.3139/146.110572.
[11] Paradis, P. F., Ishikawa, T., Yoda, S., *Int. J. Thermophys*., **26** (2005), 1031, https://doi.org/10.1007/s10765- 005-6683-y.
[12] Matson, D.M., Watanabe, M., Pottlacher, G., Lee, G.W., Fecht, H.-J. *Int. J. of Microgravity Sci. Appl.*, **33** (2016), 330301, https://doi:10.15011/ijmsa.33.330304.
[13] Lamb H, *Hydrodynamics*. Cambridge University Press, 1975, ISBN: 0 521 05515 6 - pp 450.
[14] Lord Rayleigh, *Proc. Royal Soc*. **29** (1879), 71, http://dx.doi.org/10.1098/rspl.1879.0015.
[15] Cummings, D. I., Blackburn, D. A. *J. Fluid. Mech*. **224** (1991) 395, https://doi.org/10.1017/S0022112091001817.
[16] Egry, I., Lohöfer, G., Jacobs, G. *Phys. Rev. Lett*., **75** (1995), 4043, https://doi.org/10.1103/PhysRevLett.75.4043.
[17] Etay, J., Schetelat, P., Bardet, B., Priede, J., Bojarevics, V., Pericleous, V. *High Temp. Mater. Proc.,* **27** (2008), 439, https://doi.org/10.1515/HTMP.2008.27.6.439.
[18] Priede, J., *J. Fluid Mech*. **671** (2011), 416, http://dx.doi.org/10.1017/S0022112010005781.
[19] Trinh, E. H., Thiessen, D. B., Holt, R. O., *J. Fluid Mech*., **364** (1998), 253, http://dx.doi.org/10.1017/S0022112098001153.
[20] Bojarevics V., Roy, A., Pericleous, K.A., *MAGNETOHYDRODYNAMICS*, **46** (2010), 317, http://dx.doi.org/10.22364/mhd.46.3.9.
[21] Bojarevics V., Harding, R. A., Pericleous, K., Wickings, M., *Met. Mater. Trans.*, **35B** (2004), 785, http://dx.doi.org/10.1007/s11663-004-0019-3.
[22] Hyers, R. W. *Meas. Sci. Technol*., **16** (2005), 394, http://dx.doi.org/10.1088/0957-0233/16/2/010
[23] Spitans, S., Jakovics, A., Baake, E., Nacke, B., *Met. Mater. Trans.* **B3** (2015) http://dx.doi:10.1007/s11663-015-0515-7.
[24] Bojarevics, V., Pericleous, K., *ISIJ Int.*, **43** (2003) 890, https://doi.org/10.2355/isijinternational.43.890.
[25] Prosperetti, A., *J. Fluid Mech.,* **100** (1980), 333-347. https://doi.org/10.1017/S0022112080001188.
[26] Becker, E., Hiller, W., Kowalewski, T. *J. Fluid Mech.*, **231** (1991), 189, https://doi.org/10.1017/S0022112091003361.
[27] Trinh, E. H., Zwern, A., Wang, T. G., *J. Fluid Mech.*, **115** (1982), 453, http://dx.doi.org/10.1017/S0022112082000858.
[28] Trinh, E. H., Thiessen, D. B., Holt, R. O., *J. Fluid Mech.*, **364** (1998), 253, http://dx.doi.org/10.1017/S0022112098001153.
[29] Berry, S. R., Hyers R. W., Racz, L. M. Abedian, B., *Int J. Thermophys*., **26** (2005), 1565, http://dx.doi.org/10.1007/s10765-005-8104-7.
[30] Bojarevics, V., Pericleous, K., *Int. J. Appl. Electromech.*, **44** (2014), 17, DOI: 10.323./JAE-141754.
[31] Bojarevics, V., Pericleous, K., "Modelling magnetically excited and magnetically damped liquid metal flow", CFD Modeling and Simulation in Materials, Edited by: Nastac, L., Zhang, L., Thomas, B.G., Sabau, A., El-Kaddah, N., Powell, A.C., and Combeau, H., TMS, Warrendale PA, 2012, p. 245-252. ISBN 978-1-11829-615-8
[32] Spitans, S., Jakovics, A., Baake, E., Nacke, B., Met. Mater. Trans. **B 44** (2013), 593, https://doi.org/ 10.1007/s11663-013-9809-9.
[33] Spitans, S., Baake, E., Nacke, B., Jakovics, A., *Met. Mater. Trans.*, **B 47** (2016), 522, https://doi.org/10.1007/s11663-015-0515-7.
[34] Xiao, X., Hyers, R.W., Wunderlich, R.K., Fecht, H.-J., D.M. Matson, D.M., *Appl. Phys. Lett.*, **113** (2018), 011903, http://dx.doi.org/10.1063/1.5039336.
[35] Lyubimov, D. V., Konovalov, V. V., Lyubimova, T. P., Egry, I. *J. Fluid Mech*. **677** (2011), 218, https://doi.org/10.1017/jfm.2011.78.

[36] Egry, I., Giffard, H., Schneider, S., *Meas. Sci Technol*., **16** (2005) 436, https://doi.org/10.1088/0957-0233/16/2/013.
[37] Heintzmann, P., Yang, F., Schneider, S., Lohöfer, G., Meyer, A. *Appl. Phys. Lett.***, 108** (2016) 241908-5, https://doi.org/10.1063/1.4953871.
[38] Busse, F. H. *J. Fluid Mech.*, **142** (1984), 1, https://doi.org/10.1017/S0022112084000963.
[39] Higuchi, K., Watanabe, M., Fecht, H.-J., Wunderlich, R. K. *Proc. Third Int. Symposium on Physical Sciences in Space* ISPS 2007, Nara, Japan JASMA, JAXA, **367** (2007) 217.
[40] Wunderlich, R. K., Fecht H.-J., Lohöfer, G., *Met. Mater. Trans* **B 48** (2017), 237, https://doi.org/10.1007/s11663-016-0847-y.
[41] Bracker, B., Xiao, X., Lee, J., Herlach, D., Rettenmayer, M., Reinartz, M., Burggraf, S., Matson, D. M., Hyers, R. W.,"Modeling of Fluid Flow Effects on Experiments using Electromagnetic Levitation in Reduced Gravity", Materials Processing Fundamentals 2018, Lambotte, G., Lee, J., Allanore, A., Wagstaff, S., eds., TMS 2019, Warrendale. (to appear).
[42] Schneider, S., Egry, I., Wunderlich, R., Willnecker, R., Pütz, M. *Proc. Third Int. Symp. on Physical Sciences in Space* 2007, *J. Jp. Soc. Microgravity Appl*., **25** (2008), 387.
[43] Higuchi K., H.-J. Fecht, H.-J. , Wunderlich, R. K., *Adv. Engn. Mater*., **9** (2007), 349, http://dx.doi.org/10.1002/adem.200600277.
[44] Amore, S., Valenza, F., Giuranno, D., Novakovic, R., Dalla Fontana G., Battezzati, L., Ricci, E., *J. Mater. Sci.*, **51** (2015), , https://doi.org/10.1007/s10853-015-9452-8.
[45] Quested, P. N., Brooks, R. F., Chapman, L., Morell, R., Jouseff, Y., Mills, K. C. *Mater. Sci. Technol.*, **25** (2009), 155, http://dx.doi.org/10.1179/174328408X361454.
[46] Brooks, R. F., Day, A. P., Andon, R. J. L., Chapman, L. A., Mills, K. C., Quested, P. N., *High Temp. High Press.*, **33** (2001), 73, http://dx.doi.org/10.1068/htwu139.
[47] Sato, Y., Sugisawa, K., Aoki, D., Yamamura, T. *Meas. Sci. Technol.*, **16 (**2005) 363, http://dx.doi.org/10.1088/0957-0233/16/2/006.
[48] Sato, Y., *Jpn. J. Appl. Phys.* **50** (2011) 11RD01, http://dx.doi.org/10.7567/JJAP.50.11RD01.